



A COMPREHENSIVE FLUID-SOLID INTERACTION ANALYSIS OF FINITE JOURNAL BEARINGS

Mohanad Aljanabi¹, Luay Al-Ansari², Ahmed Alhusseny³ and Adel Nasser⁴

¹ M.Sc. Student, Department of Mechanical Engineering, Faculty of Engineering, University of Kufa, Al-Najaf, Iraq. Email: mohannedaljanaby@gmail.com

² Asst. Prof., KCASE, Department of Mechanical Engineering, Faculty of Engineering, University of Kufa, Al-Najaf, Iraq. Email: Luays.alansari@uokufa.edu.iq

³ Lecturer, KCASE, Department of Mechanical Engineering, Faculty of Engineering, University of Kufa, Al-Najaf, Iraq. Email: ahmedn.alhousseini@uokufa.edu.iq; Visiting Researcher, School of Mechanical, Aerospace & Civil Engineering, University of Manchester, Manchester, UK. Email: ahmed.alhusseny@manchester.ac.uk

⁴ Senior Lecturer, School of Mechanical, Aerospace & Civil Engineering, University of Manchester, Manchester, UK. Email: a.g.nasser@manchester.ac.uk

<http://dx.doi.org/10.30572/2018/kje/100304>

ABSTRACT

As key elements in plenty of rotating machinery, the elastohydrodynamic performance of journal bearings should be carefully checked in light of the design and operating parameters considered. This first part of the current study aims to numerically analyse the operation of journal bearings under alignment conditions. In the fluid-solid interaction analysis conducted, the lubricant flow field is solved using the finite volume method. Based on finite elements strategy, a structural analysis is then implemented to the solid bearing using the pressure distribution computed earlier on its inner surface. A wide range of operating conditions has been considered including the eccentricity ratio ($0.1 \leq \varepsilon \leq 0.9$), bearing length-diameter ratio ($0.8 \leq L/D \leq 2$), and rotation speed ($4,000 \leq N \leq 10,000$ rpm). Three principal categories of operational quantities have inspected, namely; the lubricant pressure distribution, overall performance parameters, and structural aftereffects. Among all the parameters examined, the eccentricity ratio is the most influential one on the performance of journal bearings. As it increases with applying heavier loads, a significant rise occurs in each of the friction force, power loss, stress levels, and deformation on the inner surface of the bearing. The bearing length and rotation speed, on the other hand, affect the bearing performance as well, but to a less extent.

KEYWORDS: Fluid-Solid Interaction; Numerical Analysis; Elasto-hydrodynamic Performance; Journal Bearing

1. INTRODUCTION

Journal bearings are essentially incorporated in all types of machinery involving rotating parts. Due to their potentials to suppress a variety of exciting loads influencing the rotational elements, journal bearings have a direct impact on the dynamic behaviour of rotating shafts. Demands of seeking high productivity in industrial sectors while keeping compactness of the rotating machinery used are usually achieved with not only the cost of raising the rotational speed and bearing loads, but it also promotes the severity and variety of exciting forces generated. Therefore, a tremendous attention has been paid to the role played by such a sort of bearings particularly due to the desire to design rotating machinery with limited vibration levels and high operational reliability.

One of the pioneer works in this context was the study presented by (DuBois and Ocvirk, 1952) for a short bearing, where the Reynolds equation was analytically solved for the pressure distribution. The results obtained were validated against the pressure data measured experimentally. However, the analysis has not agreed well with the experimentations conducted. Later on, a series of investigations (Raimondi and Boyd, 1958a, 1958b, 1958c) were presented in the context of analysis and design of finite journal bearings, where the Reynolds equation was solved numerically for the pressure distribution. For various bearing arcs, the load capacity was predicted, but only for a single value of bearing length, i.e. $L/D=1$. Afterwards, an analytical solution for the Reynolds equation was presented by (Donaldson, 1967). In this investigation, the lubricant was assumed to be Newtonian and incompressible under laminar flow regime. Both the shaft and bearing were considered to be rigid cylinders aligned together. The solution obtained is valid for finite journal bearings, where pressure distribution and load capacity can be estimated.

In their three-dimensional numerical investigation, (Oh and Huebner, 1973) used the finite elements method to analyse the performance of finite journal bearings taking into account the effect of the bearing deformation on the film pressure distribution. The comparison conducted between the results computed and the corresponding experimental data inferred that a bench of design parameters should be considered altogether in order to come with meaningful perspective. The elastic deformation of a cylindrical bearing was numerically predicted by (Jain, Sinhasan and Singh, 1982) using the finite elements method. The Reynolds equation was firstly solved for the pressure distribution and then the three-dimensionally linear elasticity equations were solved for the deformation vector. The deformation resulted over the inner surface of the bearing was compared for two materials having different Poisson's ratios. It was

found that the load supported is reduced while increasing the Poisson's ratio resulting in a reduction in the eccentricity generated. However, the data obtained were limited for a bearing with length $L/D = 1$ and eccentricity $\varepsilon = 0.6$. Similarly, (Khonsari and Wang, 1991) solved the lubricant field numerically for the pressure distribution, but with taking the thermal effects into account. In this work, the thermo-elastohydrodynamic phenomenon was explored for the first time; however, combining the elastic and thermal influences together requires paying more attention to avoid meaningless conclusions.

The elastohydrodynamic performance of journal bearing operating in diesel engines was investigated numerically by (Okamoto, Hanahashi and Katagiri, 1999). Bearings of different lengths were examined, where it was observed that shorter bearings are subjected to lower load capacity. However, an extreme reduction in the bearing length was found to promote the lubricant shear resistance, and hence, results in higher power loss.

Using water as a lubricant in combination with a rubber bearing was examined experimentally and numerically by (Cabrera et al., 2005). It was found that using rubber rather than rigid materials results in a quite different pressure distribution, where significant deformation is measured despite the relatively low lubricant pressure produced. The impact of using a non-Newtonian lubricant was numerically investigated by (Gertzos, Nikolakopoulos and Papadopoulos, 2008) using the finite elements method. The working fluid is considered to behave like a Bingham fluid, and hence, Bingham plastic model is employed to describe the behavior of the non-Newtonian fluid flow. The numerically computed data were validated against previously experimental results, where good agreement has been found. However, nor the stresses generated, neither the deformation resulted were considered in this work.

The fluid-solid interaction in a journal bearing system was numerically analysed by (Liu et al., 2010). The solid dynamic response was predicted by means of the fluid flow behavior in the film region. It was found that the bearing system is quite sensitive to the elastic deformation generated, especially when polymers-based materials are used. Moreover, dynamic loads were found to be of obvious impact on the rotor-bearing system.

An exact solution was later derived by (Sfyris and Chasalevris, 2012) for the Reynolds equation by using the variables separation method. The solutions were presented for static and dynamic conditions and valid for both the infinitely long and short bearings. This investigation was further extended later to compute the carrying load analytically (Chasalevris and Sfyris, 2013). Using the formulations presented in both studies, the location of maximum pressure, stiffness and damping coefficients can be estimated.

Based on CFD analysis, the film cavitation in journal bearings under thermal effects was studied by (Lin et al., 2013). The rotation speed was found to play a dominant role in augmenting the lubricant temperature and promoting the cavitation formation, which implies serious constraints on the design of highly-rotating journals. The isothermal operation of journal bearings was investigated numerically by (Wodtke, Olszewski and Wasilczuk, 2013), where the formation of cavitation was predicted in terms of the operating conditions examined. Unlike the case of water-lubricated journal bearings, it was observed that the negative lubricant pressure has no obvious impact on the performance of oil-lubricated bearings. This outcome was attributed to the high maximum-to-minimum pressure ratio in the case of oil-lubricated bearings compared to the corresponding water-lubricated ones. In a similar context, cavitation phenomenon was numerically predicted by (Gao et al., 2014) and compared for water- and oil-lubricated journal bearings. The numerically computed results were verified against the corresponding experimentally measured data, where a design reference was presented to select the initial dimensions of water-lubricated bearings.

Overall, there are two categories regarding the analyses conducted for the lubricant performance in journal bearings; static and dynamic analysis. In the first one, the analysis is based on assuming that the shaft is shifted in a certain direction. This displacement is usually given as a dimensionless ratio called the eccentricity. The other sort, on the other hand, is known as the dynamic analysis, in which the journal is shifted and misaligned due to the loads applied to the shaft itself. The current project is aimed to present a static analysis for the elastohydrodynamic performance of aligned journal bearings under various geometric and operating conditions; where to the best of our knowledge, no such a comprehensively detailed investigation has yet been presented.

2. MATHEMATICAL FORMULATION

The mathematical formulation can be divided into two main parts. The first is the film flow domain, while the other is the solid structure of the bearing. The journal bearing simulated, as shown in Fig. 1, is composed of two eccentric and aligned cylinders of length L , while the outer radius of each of the journal and bearing is 50 and 55 mm, respectively. The clearance between the rotating shaft and the inner surface of the bearing is chosen to be 0.152 mm (Ferron, Frene and Boncompain, 1983).

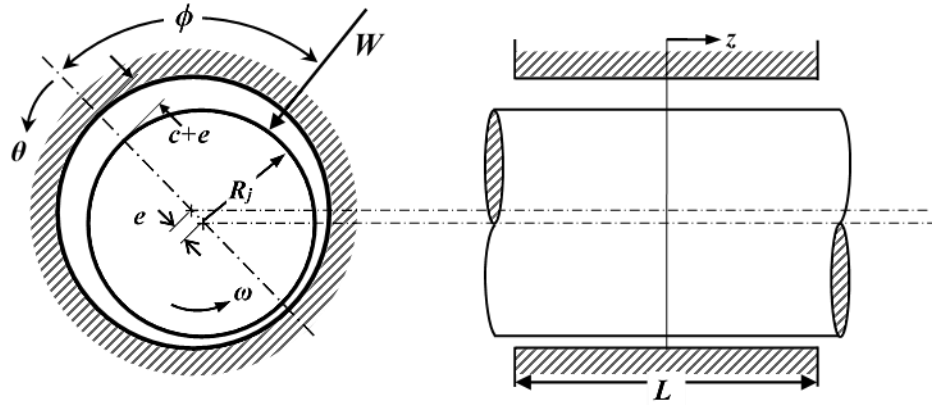


Fig. 1 the cross section of full journal bearing.

The three dimensional lubricant flow through the clearance is assumed to be steady, incompressible, and laminar. The lubricant used is ISO VG32 oil having density of 860 kg/m^3 , while its dynamic viscosity is $0.0277 \text{ Pa}\cdot\text{sec}$ (Dobrica and Fillon, 2012). Thus, the partial differential equations governing the conservation of mass and momentum for the film layer are as follows (Versteeg and Malalasekera, 2007):

$$\frac{\partial u}{\partial x} + \frac{\partial v}{\partial y} + \frac{\partial w}{\partial z} = 0 \quad 1$$

$$\rho_f \left(u \frac{\partial u}{\partial x} + v \frac{\partial u}{\partial y} + w \frac{\partial u}{\partial z} \right) = -\frac{\partial p}{\partial x} + \mu \left(\frac{\partial^2 u}{\partial x^2} + \frac{\partial^2 u}{\partial y^2} + \frac{\partial^2 u}{\partial z^2} \right) \quad 2$$

$$\rho_f \left(u \frac{\partial v}{\partial x} + v \frac{\partial v}{\partial y} + w \frac{\partial v}{\partial z} \right) = -\frac{\partial p}{\partial y} + \mu \left(\frac{\partial^2 v}{\partial x^2} + \frac{\partial^2 v}{\partial y^2} + \frac{\partial^2 v}{\partial z^2} \right) \quad 3$$

$$\rho_f \left(u \frac{\partial w}{\partial x} + v \frac{\partial w}{\partial y} + w \frac{\partial w}{\partial z} \right) = -\frac{\partial p}{\partial z} + \mu \left(\frac{\partial^2 w}{\partial x^2} + \frac{\partial^2 w}{\partial y^2} + \frac{\partial^2 w}{\partial z^2} \right) \quad 4$$

On the other hand, the bearing structure is formed of stainless steel having density of 7850 kg/m^3 , modulus of elasticity 210 GPa , Poisson ratio 0.3 , and yield strength of 200 GPa . Thus, the partial differential equation governing the stress distribution in the solid bearing is based on the Newton's second law of motion, as follows:

$$\rho_s \ddot{\mathbf{\delta}} = \nabla \cdot \boldsymbol{\sigma}_s + \mathbf{f}_s \quad 5$$

As the film flow is surrounded by solid walls, no-slip occurs on each of the journal and bearing surfaces. This implies that the lubricant particles in the vicinity of the rotating journal always have zero relative velocity with the rotating shaft to maintain the non-slip condition. Moreover, the condition at the sidewalls bounding the film field is assumed to be at atmospheric state, i.e. zero gauge pressure.

$$\left. \begin{array}{ll} \text{at } r = R_j : & u = \omega R_j, \quad v = w = 0 \\ \text{at } r = R_{bi} : & u = v = w = 0 \\ \text{at } z = \pm L/2 : & p = 0 \end{array} \right\} \quad 6$$

The solid bearing, on the other hand, is exposed to an internal pressure load resulting from the lubricant flow field, while the external wall is considered to be fixed. Furthermore, the side boundaries are maintained free-loaded.

$$\left. \begin{array}{ll} \text{at } r = R_{bi} : & \mathbf{F} = p(\theta, z) dA \\ \text{at } r = R_{bo} : & \delta = 0 \\ z = \pm L/2 : & \mathbf{F} = 0 \end{array} \right\} \quad 7$$

3. SOLUTION PROCEDURE

As mentioned earlier, the system investigated is composed of two regions, i.e. fluid and solid, linked through a fluid-solid interface. So, the partial differential equations governing the fluid flow and stress propagation are discretised through different methods, i.e. finite volumes and finite elements method, respectively. Based on the second-order upwind differencing scheme, the discretised equations for the lubricant flow field have been solved following the SIMPLE algorithm (Versteeg and Malalasekera, 2007).

The mesh used to solve the system is built using ANSYS Meshing software, where hexahedral cells are used for both the fluid and solid zones, as illustrated in Fig. 2. Grid dependency was checked for three sets of film mesh to examine the sensitivity of the results computed to the number of grid divisions along each of the physical coordinates, i.e. radial n_i , circumferential n_j , and axial n_k . In general, it has been observed that the number of the divisions along the radial direction n_i dominates the accuracy of the solution obtained unlike the number of divisions along the other two directions, i.e. n_j or n_k , which have no noticeable impact. As shown in Table 1, increasing the grid divisions along the radial coordinate improves the results accuracy significantly until the error becomes quite marginal between $n_i=6$ & 7, which is about 0.9434%. Thus, using only six divisions across the clearance space sounds quite reasonable. As preceded, the increase in the grid divisions along either the circumferential or axial coordinate results in no obvious change in the maximum pressure applied on the bearing surface. However, the circumference and axial length have been respectively divided into 360 and 60 elements to avoid having extremely slim elements, or in other words, keeping reasonable aspect ratios for

the elements generated. Accordingly, a grid size of ($n_i=6$, $n_j=360$, $n_k=60$) is considered for all the simulations to be carried out in the current investigation.

Table 1. Grid sensitivity for $L/D=1$, $N=10,000$ rpm, and $\varepsilon=0.5$.

Effect of the radial divisions (n_j, n_k)=(360, 60)		
n_i	P_{max} (MPa)	Error (%)
2	2.82	-----
3	4.05	30.37037
4	4.70	13.82979
5	5.05	6.930693
6	5.25	3.809524
7	5.30	0.943396

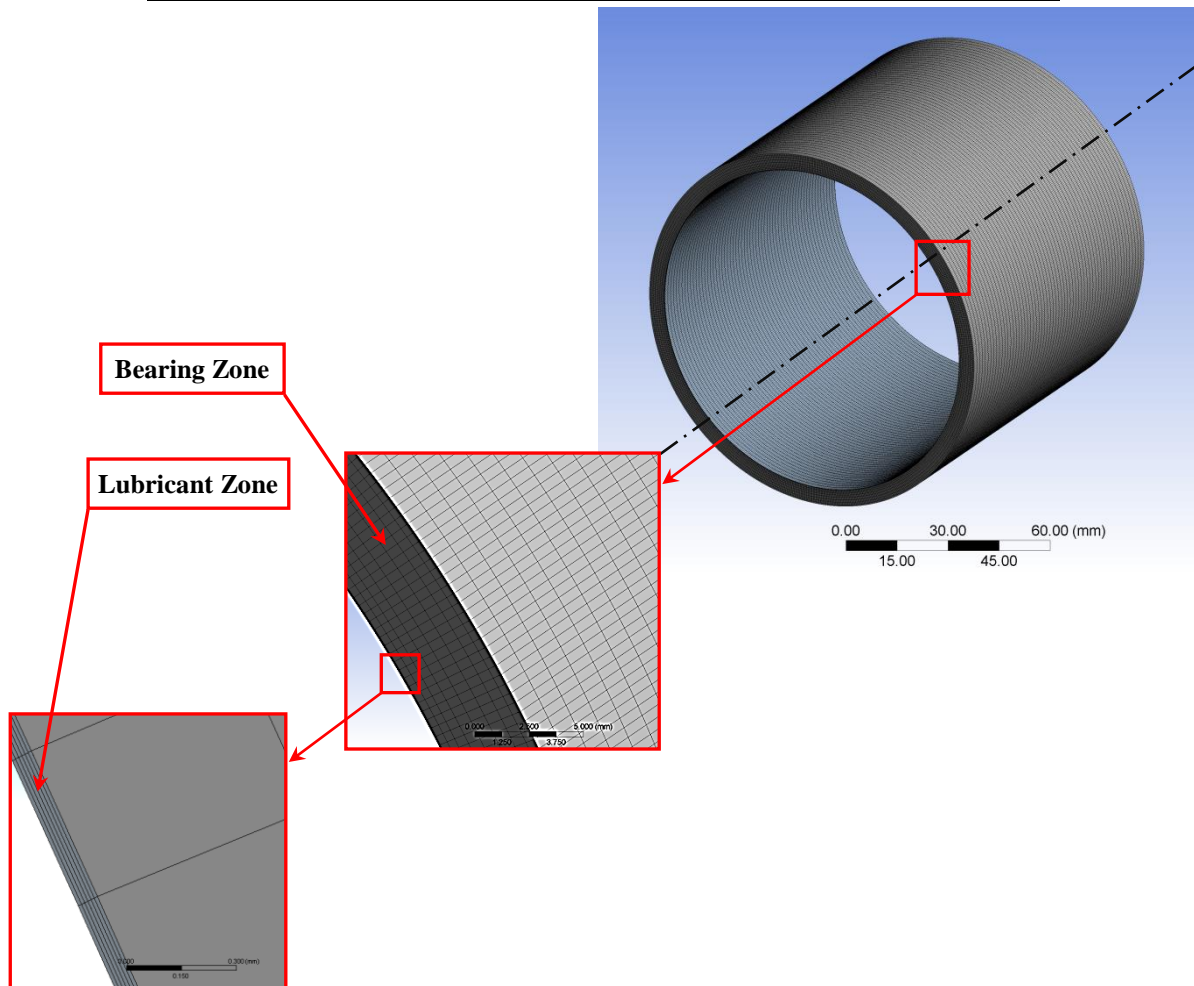


Fig. 2. Geometry for Bearing and fluid film mesh by hexahedral cells.

The lubricant flow field is iteratively solved using the well-known ANSYS Fluent commercial code, which is linked to ANSYS Static Structural code to predict the stress propagation and the deformation resulted. To verify the reliability of the numerical methodology used, the numerically computed results need to be validated. The currently simulated FSI data were compared with the experimentally measured data by (Wada, Hayashi and Haga, 1974) and also validated against the analytical approximation established by (Sfyris and Chasalevris, 2012), were the circumferential distribution of dimensionless pressure, defined as $P = p c^2 / \mu \omega R_j^2$, was compared as shown in Fig. 3 for a wide range of eccentricities and bearing lengths. In general, the currently computed data are in a good agreement with the analytically predicted data, where the maximum deviation was about 7%. This slight mismatch might be attributed to the inaccuracy in the measurements techniques used in the experiments and the approximations followed to obtain the analytical solution. Overall, this comparison revealed the validity of the current computational simulation.

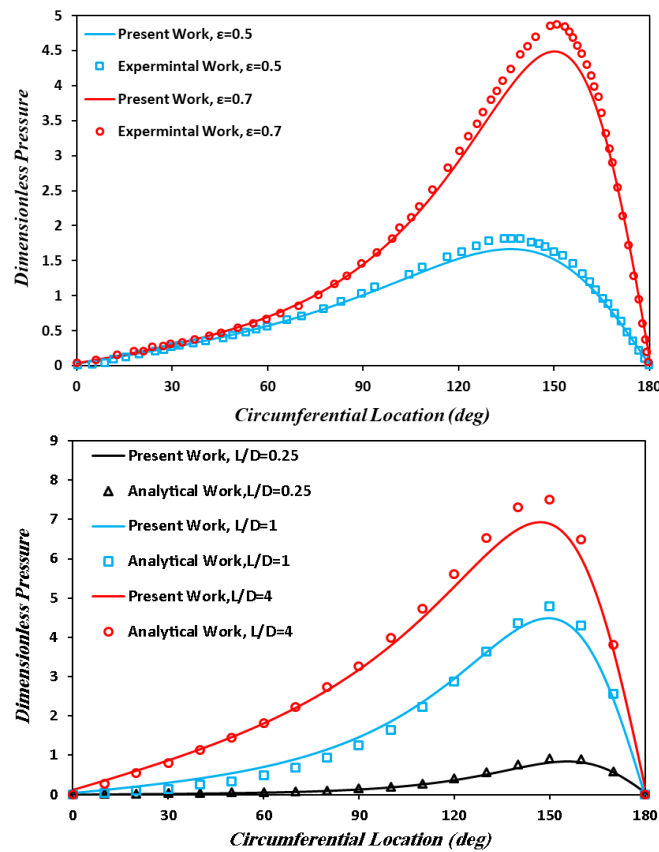


Fig. 3 Comparison with the dimensionless pressure experimentally measured by (Wada, Hayashi and Haga, 1974) for various eccentricities (left) and the analytically predicted by (Sfyris and Chasalevris, 2012) for various bearing lengths (right).

4. RESULTS

The results acquired have been computed for a wide range of design parameters including the eccentricity ratio ($0.1 \leq \varepsilon \leq 0.9$), bearing length-diameter ratio ($0.8 \leq L/D \leq 2$), and rotation speed ($4,000 \leq N \leq 10,000$ rpm).

4.1 Impact of design parameters on the lubricant film

Among the multiple parameters influencing the performance of journal bearings is the shaft location. When the journal starts to rotate, the shaft location will oscillate around the bearing center until reaching its final position when equilibrium is acquired between the load applied by the shaft and the pressure exerted on the lubricant film. As a result of the load applied combined with rotation, the journal is shifted down generating an eccentricity between the centres of the shaft and the bearing surrounding it. This leads to narrowing the flow path at the lowest point along the circumference, as shown in Fig. 4. Hence, the flow field is significantly altered due to the converging-diverging area formed within the lubricant film, which affects the pressure distribution as shown in Fig. 5. According to Fig. 4, the lubricant film thickness at the lowest position is reduced while increasing the eccentricity ratio, and consequently, the exerted pressure over the lubricant particles there is significantly augmented along with shifting the angle of attitude downwards, as shown in Fig. 5. This phenomena can be demonstrated more clearly in Fig. 6, which illustrates the dimensionless pressure profile along the circumference at $Z=0$ for various length and eccentricity ratios. It is apparent, as preceded, that the area subjected to maximum pressure values is shifted downwards while increased the eccentricity ratio.

Another key factor influencing the pressure distribution is the bearing length. As shown in Fig. 6, the pressure is, in general, increased with the bearing length due to the increase occurs in the overall force acting on the film layer, which is attributed to the increase in the contact area between the rotating journal and the lubricant surrounding it.

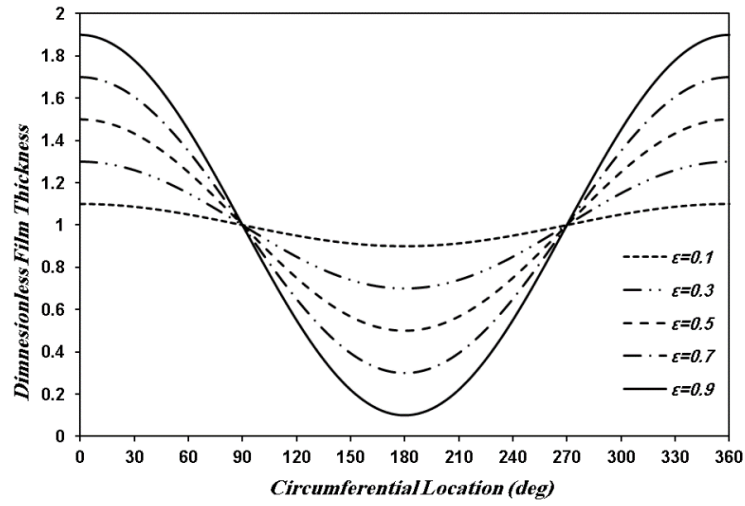


Fig. 4. Circumferential variation of dimensionless film thickness for various eccentricity ratios.

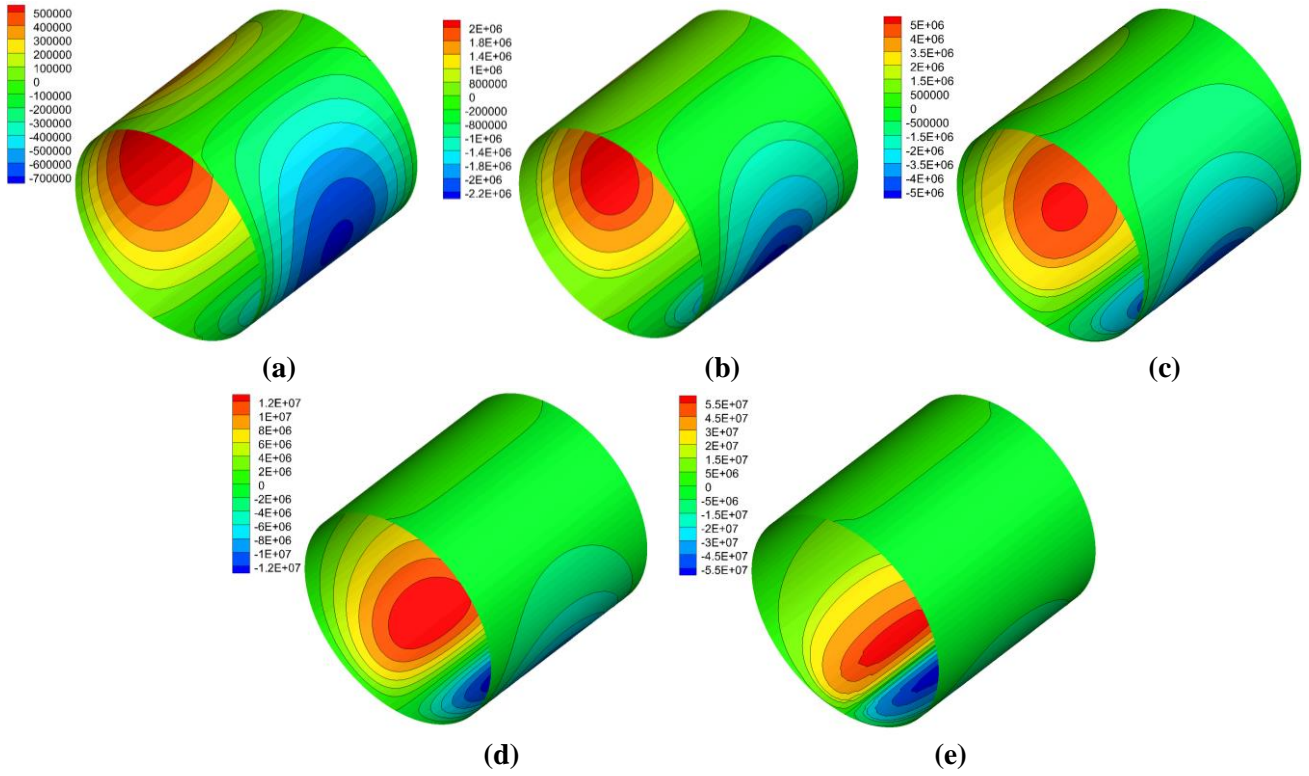


Fig. 5. Effect of eccentricity ratio on the lubricant pressure applied on the bearing surface for $L/D=1$ and $N=10,000$ rpm; a) $\varepsilon=0.1$, b) $\varepsilon=0.3$, c) $\varepsilon=0.5$, d) $\varepsilon=0.7$, and e) $\varepsilon=0.9$.

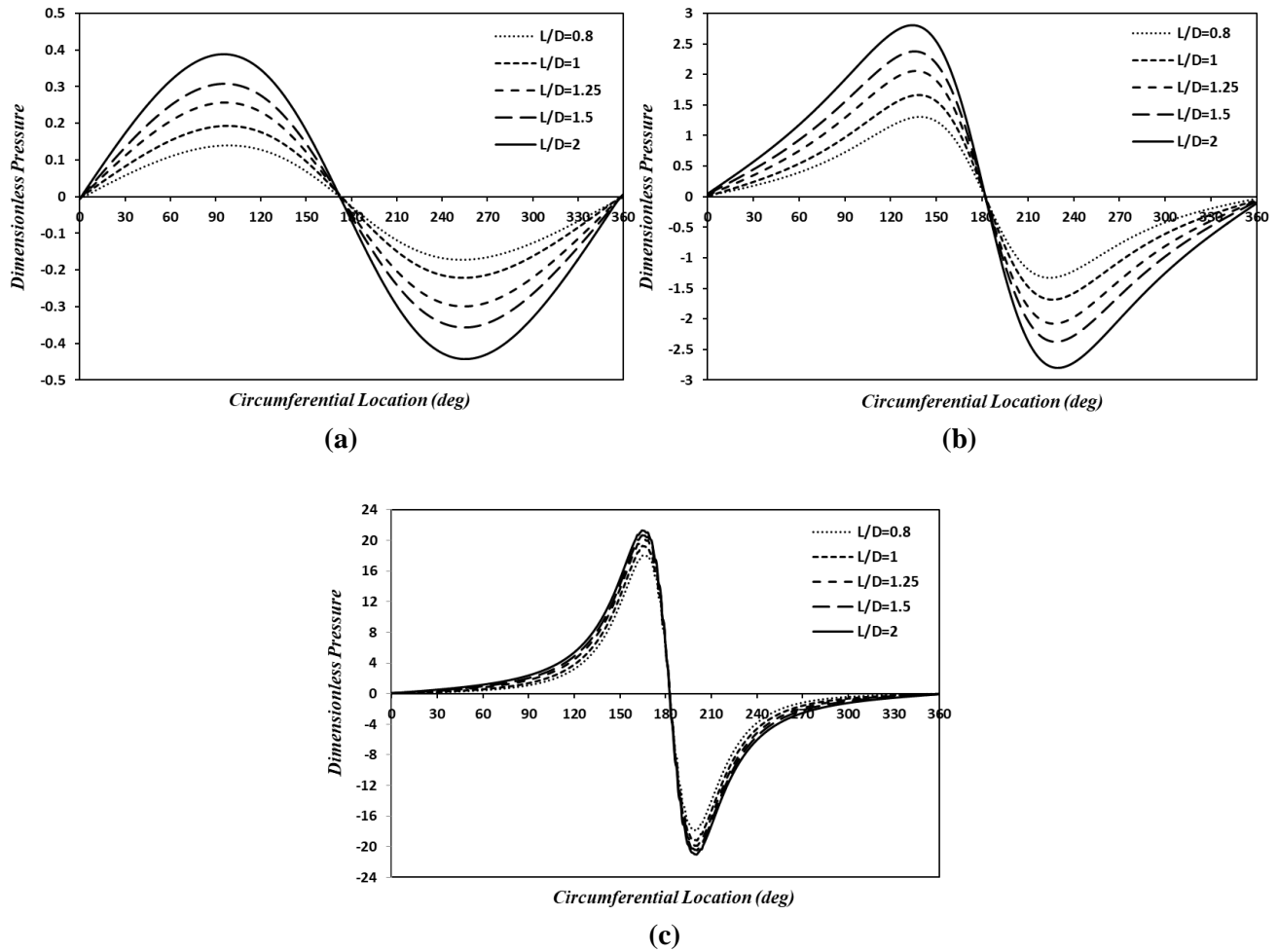


Fig. 6. Effect of bearing length on dimensionless pressure distribution along the circumference at $Z=0$ for various eccentricity ratios; a) $\varepsilon=0.1$, b) $\varepsilon=0.5$ and c) $\varepsilon=0.9$

4.2 Impact of design parameters on the overall performance of journal bearings

The performance of journal bearings is assessed through looking at the consequential effects due to changing some quantities related to their operation. The most important parameter in selecting a journal bearing operating at specific conditions is the load acting on it, which is called the carrying load and defined as $(W = \iint_A p \, dA)$. As shown in Fig. 7, the load carried by the bearing is augmented with the eccentricity ratio. Furthermore, the journal rotating with higher speed causes heavier load due to the increase in the centrifugal force. Similarly, the load applied for longer bearings is increased as well due to the larger surface area exposed to the lubricant pressure applied.

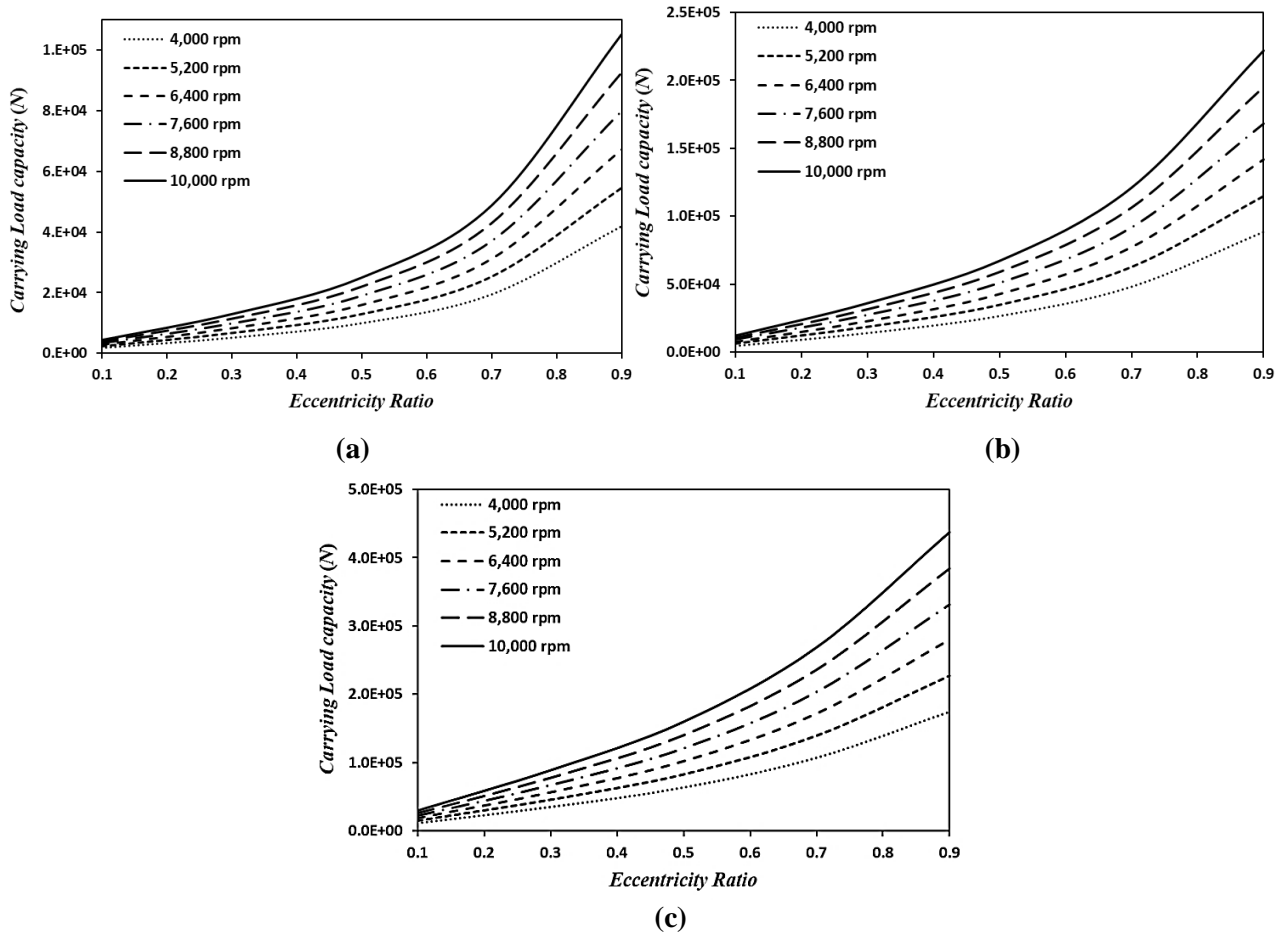


Fig. 7. Influence of eccentricity ratio on the carrying load for various rotation speeds at;
a) $L/D=0.8$, b) $L/D=1.25$ and c) $L/D=2$.

Sommerfeld number, which is defined as $S_n = \mu U L (R_j / c)^2 / \pi W$, is a dimensionless quantity useful in bearings design. It involves the combined effects of bearing dimensions, friction force, rotation speed, and the load applied. Hence, for a journal bearing with given geometric and operating conditions, it indicates the operational status of a film-lubricated bearing. For example, the decrease of Sommerfeld number indicates that the load applied has been increased and the eccentricity as well.

The friction force, which is directly proportional to load applied and rotation speed, can be defined as $F_i = \iint_A \tau_i dA$, where i stands for the surface where the friction force acts on, which is either the journal surface or the inner surface of the bearing. As the friction force acting on the journal surface represents the source of film rotational motion, its value is higher than it is on the inner surface of the bearing. Therefore, the coefficient of friction, wherever it is mentioned in the text, characterises the friction on the journal surface only. The coefficient of friction, which represents the ratio of the friction force to the load applied, is reduced with the

bearing length due to the influential increase in the load applied compared to the simultaneously corresponding increase in the friction force, as shown in Fig. 8. In general, the friction coefficient of friction increases with Sommerfeld number, or in other words, with the reduction in the load applied and the eccentricity resulting from it. However, this trend is reversed for long bearings and low Sommerfeld number, i.e. $L/D \geq 1$ and $S_n \leq 0.04$, where the friction coefficient tends to decrease slightly with Sommerfeld number. This is due to the extremely narrow flow path, which in turns results in promoting the role played by the friction force compared to the simultaneous load applied.

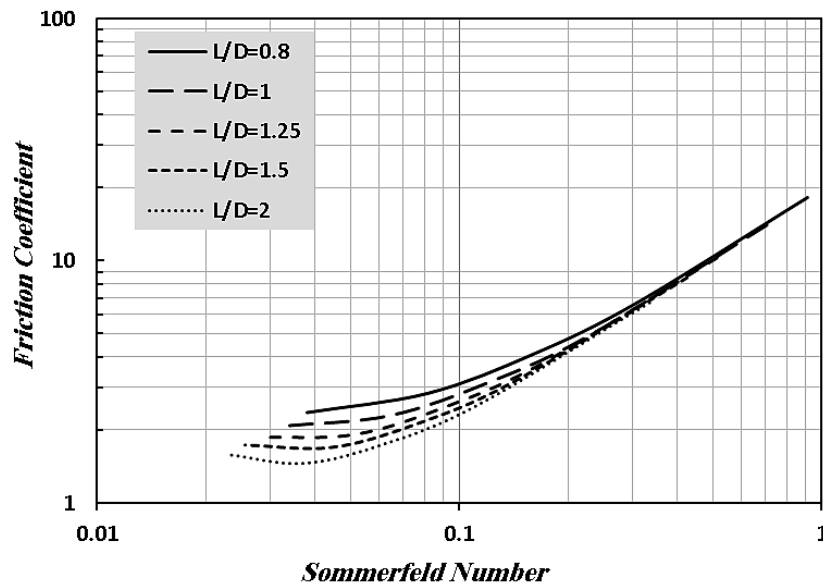


Fig. 8. Variation of friction coefficient with Sommerfeld number for various bearing lengths.

While the journal rotates inside the bearing, an amount of the energy to be transported is lost due to friction. As clearly demonstrated by Fig. 9, power loss is directly proportional to each of the friction force and the rotation speed and defined as $H = F_f U_j$. It increases with the rotation speed due to the increase in both the friction force and tangential speed of the journal U_j . Also, it is increased with the bearing length due to the increase of the surface area subjected to friction with the lubricant particles. Similar outcome is observed while increasing the eccentricity ratio. This is due to the reduction occurs in the thickness of lubricant layer resulting in increasing the friction there.

4.3 Impact of design parameters on the elastic performance of journal bearings

The bearing is stressed as a result of the pressure exerted by the lubricant film on its inner surface. The stress propagation into the solid bearing, which is a reflection to the pressure distribution over its inner surface, is illustrated in Fig. 10. As the pressure increases with the

eccentricity ratio, the stress generated on the inner surface of the bearing is increased as well. To examine the stress response to the design parameters selected, the maximum stress is plotted in Fig. 11 as a function to the rotation speed and bearing length for various eccentricity ratios. In general, shifting the journal downwards, or in other words increasing the eccentricity ratio, results in higher levels of the stress generated due to the augmentation of the lubricant pressure applied to the inner surface of the bearing. For similar reasons, the maximum stress is raised as well while increasing the bearing length. However, a close look at the combined effects of the eccentricity and length ratios reveals that the role played by the length ratio is reduced with increasing the eccentricity ratio. This is ought to the increasing dominance of increasing the eccentricity ratio compared to corresponding role played by the increase in the bearing length. Moreover, it is observed that while the rotation speed is increased, the bearing is further stressed as a result of the augmentation in the carrying load applied.

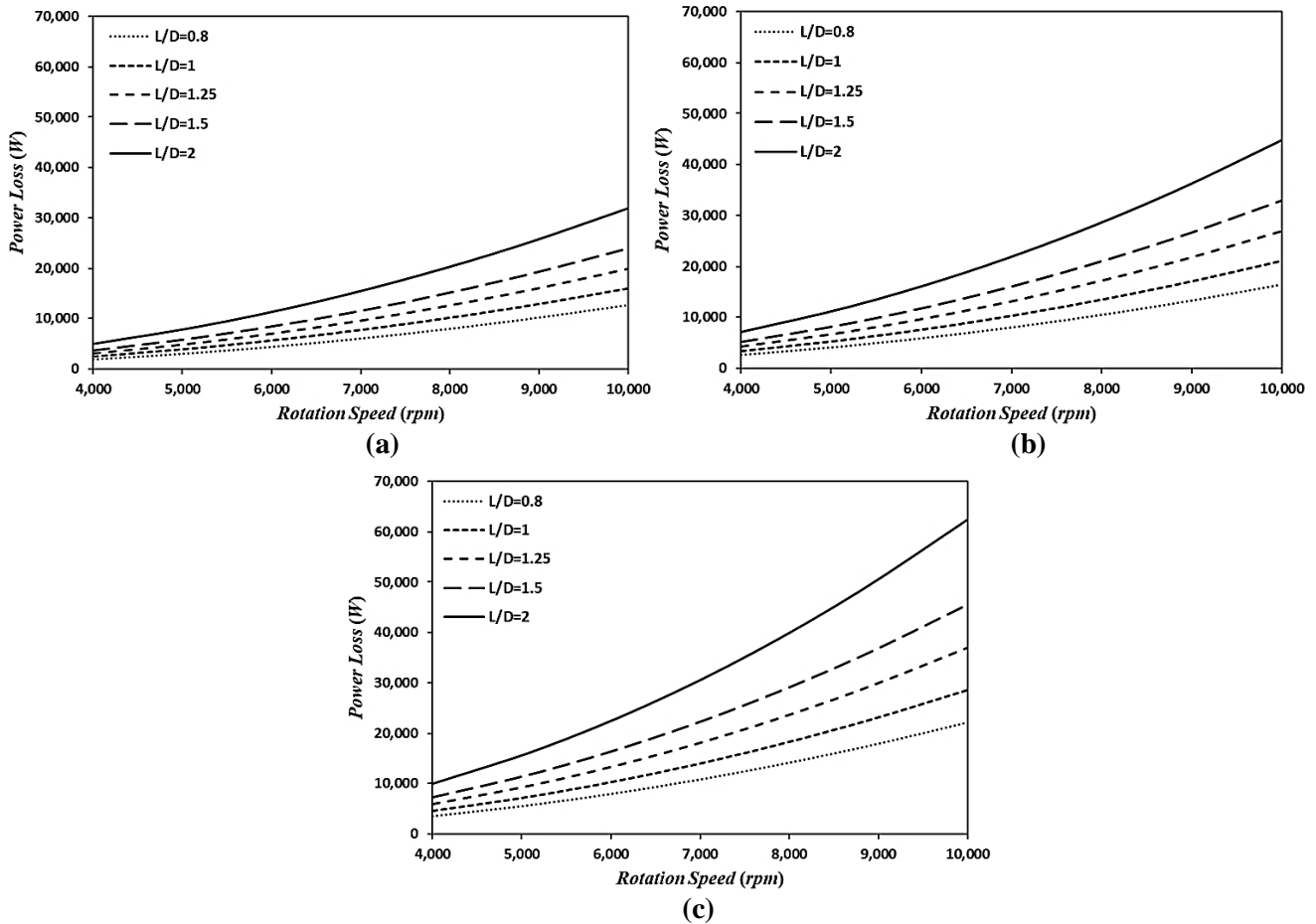


Fig. 9. Influence of rotation speed on the power lost for various bearing lengths at; a) $\varepsilon=0.1$, b) $\varepsilon=0.5$ and c) $\varepsilon=0.9$.

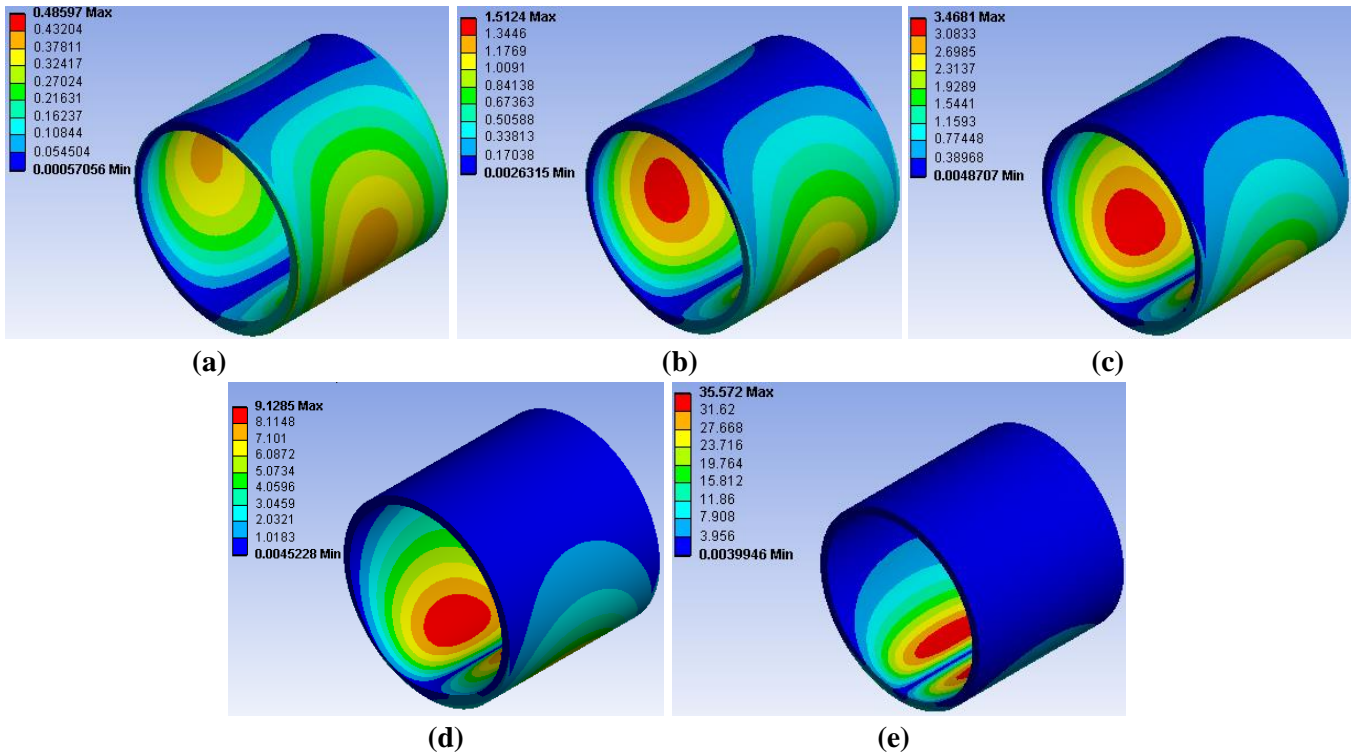


Fig. 10. Effect of eccentricity ratio on the stress propagation through a bearing of $L/D=1$ and $N=10,000$ rpm; a) $\epsilon=0.1$, b) $\epsilon=0.3$, c) $\epsilon=0.5$, d) $\epsilon=0.7$, and e) $\epsilon=0.9$.

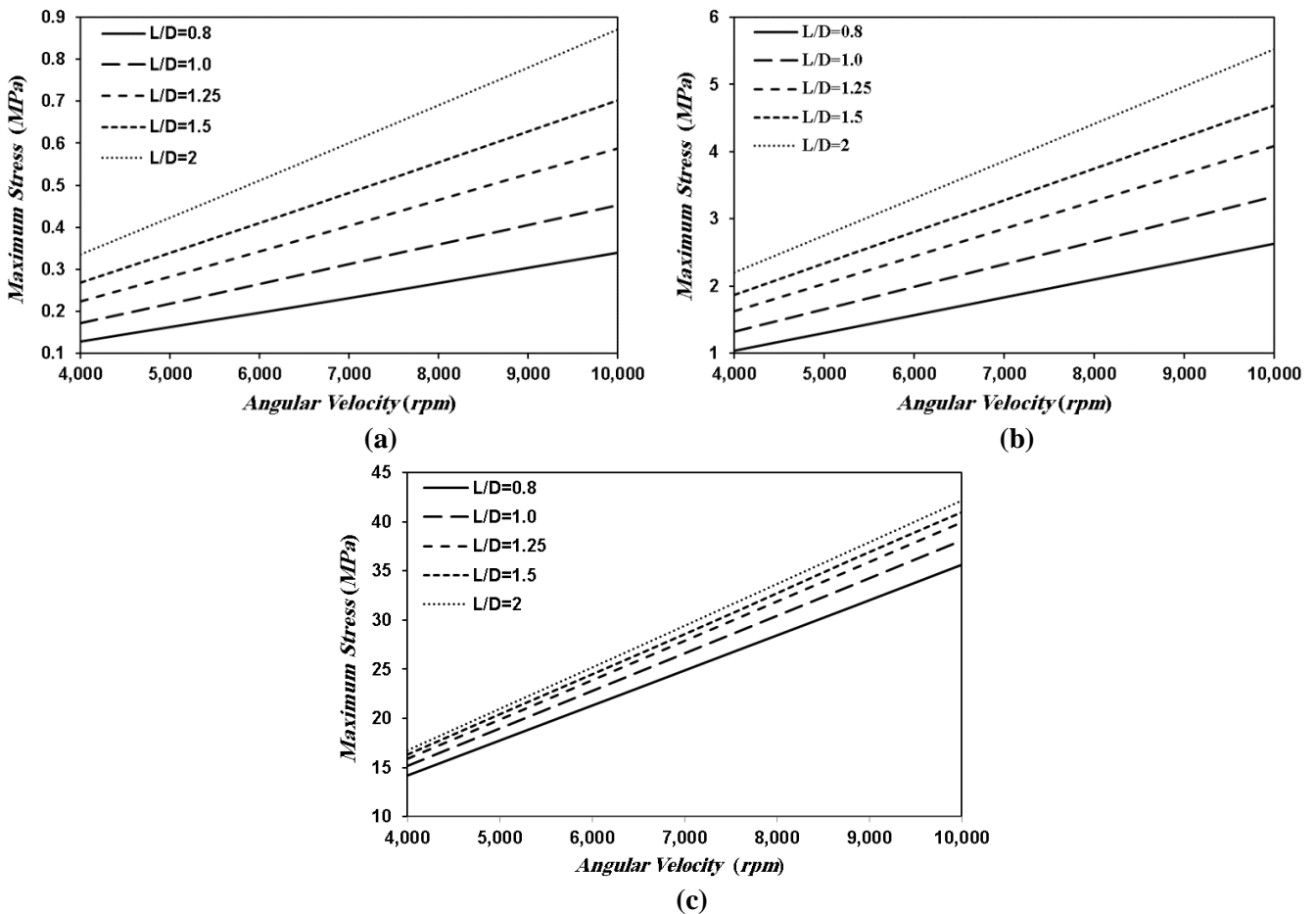


Fig. 11. Influence of rotation speed on the maximum stress for various bearing lengths at; a) $\epsilon=0.1$, b) $\epsilon=0.5$ and c) $\epsilon=0.9$.

As the bearing is stressed due to the load exerted over its inner surface, a deformation is generated as a result of the non-uniform distribution of the lubricant pressure over that surface. The three-dimensional distribution of the deformation generated is illustrated in Fig. 12 for various values of eccentricity ratio. As the deformation is an expected outcome of the stress applied, its values are raised with the increase in the eccentricity ratio, as demonstrated earlier in Fig. 11. The deformation is increased as well with the increase in both the rotational speed and the bearing length, as demonstrated by Fig. 13. Among these parameters, the effect of the eccentricity is the most dominant one. On the other hand, the influence of increasing the bearing length on the deformation resulted seems to be marginal. This is attributed to the fact that the material used in the tested bearing, i.e. stainless steel, has a high modulus of elasticity (Khonsari and Wang, 1991).

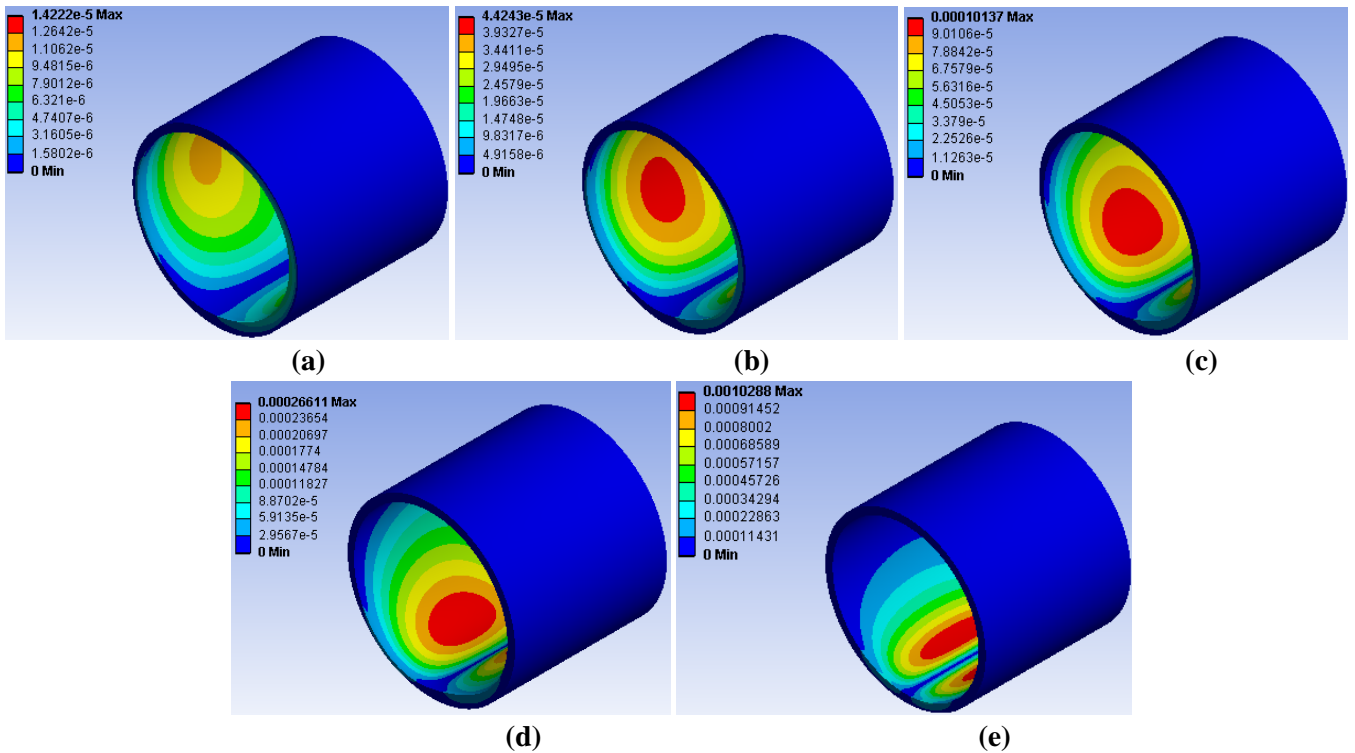


Fig. 12. Effect of eccentricity ratio on the deformation resulted on the inner surface of a bearing having $L/D=1$ and rotating at $N=10,000$ rpm; a) $\epsilon=0.1$, b) $\epsilon=0.3$, c) $\epsilon=0.5$, d) $\epsilon=0.7$, and e) $\epsilon=0.9$.

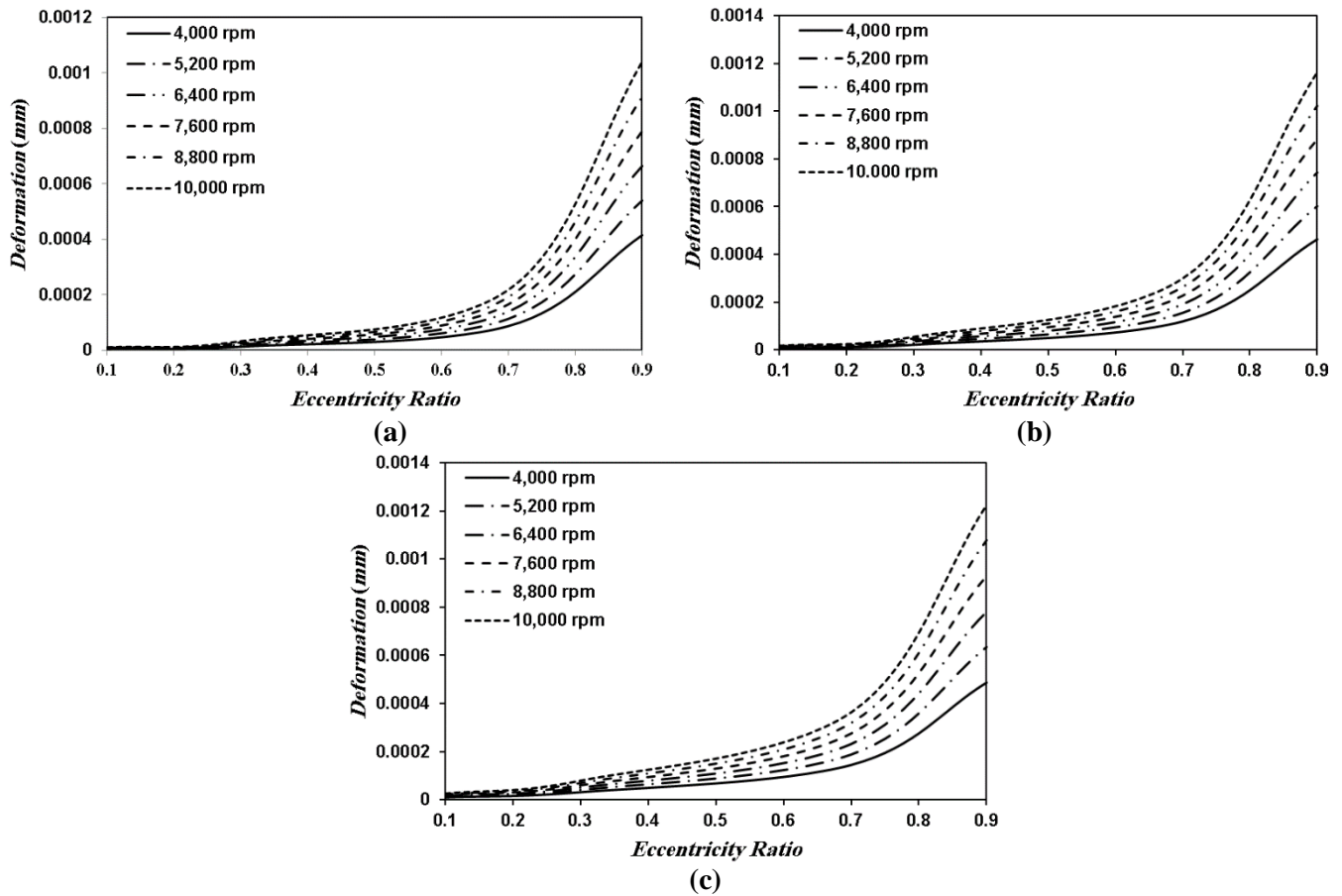


Fig. 13. Influence of eccentricity ratio on the deformation resulted for various rotation speeds at;
a) $L/D=0.8$, b) $L/D=1.25$ and c) $L/D=2$.

5. CONCLUSIONS

In present work, the elasto-hydrodynamic performance of aligned journal bearings is numerically examined for various operating conditions. The finite volumes method has been employed to solve the lubricant flow, which is considered steady, incompressible, and laminar. The structural analysis, on the other hand, has been conducted using the finite elements method, where the bearing is stressed due to the lubricant pressure applied over its inner surface. To sum up, the following remarks have been concluded:

1. The FSI technique followed in this work is efficient enough to predict the performance of finite journal bearings accurately.
2. While the bearing length increases, the load capacity of a journal bearing is increased for a particular eccentricity ratio, i.e. larger applied load can be carried. This leads to a significant increase in the maximum pressure generated within the lubricant field as well as the deformation and stresses within the bearing.

3. While the eccentricity ratio increases as a result of increasing the load applied, the position of the maximum and minimum pressure are shifted towards the position of minimum film thickness. Also, as the value of maximum and minimum pressures increase, the deformations and stresses are augmented as well.
4. When the speed of the shaft increases, the carrying load capacity increases for a particular eccentricity ratio due to the increase in the lubricant pressure. This results in a considerable augmentation of both the stresses and deformations within the bearing.
5. The coefficient of friction, in general, increases with Sommerfeld number, or in other words, with the reduction in the load applied and the eccentricity resulting from it.

6. ACKNOWLEDGEMENTS

The authors like to acknowledge the role played by the University of Manchester in providing the IT resources required to conduct this project. Also, the support provided by the *KCASE* “Kufa Centre for Advanced Simulation in Engineering” is greatly appreciated.

7. REFERENCES

- Cabrera, D. L. *et al.* (2005) ‘Film pressure distribution in water-lubricated rubber journal bearings’, *J.Engineering Tribology*, 219(2), pp. 125–132. doi: 10.1243/135065005X9754.
- Chasalevris, A. and Sfyris, D. (2013) ‘Evaluation of the finite journal bearing characteristics, using the exact analytical solution of the Reynolds equation’, *Tribology International*. Elsevier, 57, pp. 216–234. doi: 10.1016/j.triboint.2012.08.011.
- Dobrica, M. B. and Fillon, M. (2012) ‘Performance degradation in scratched journal bearings’, *Tribology International*. Elsevier, 51, pp. 1–10. doi: 10.1016/j.triboint.2012.02.003.
- Donaldson, R. R. (1967) ‘A General Solution of Reynolds’ Equation for a Full Finite Journal Bearing’, *Journal of Lubrication Technology*, 89(2), pp. 203–210.
- DuBois, G. B. and Ocvirk, F. W. (1952) *Analytical Derivation and Experimental Evaluation of Short-Bearing Approximation for Full Journal Bearings*.
- Ferron, J., Frene, J. and Boncompain, R. (1983) ‘A Study of the Thermohydrodynamic Performance of a Plain Journal Bearing Comparison Between Theory and Experiments’, *Journal of Lubrication Technology*, 105(3), p. 422. doi: 10.1115/1.3254632.
- Gao, G. *et al.* (2014) ‘Numerical analysis of plain journal bearing under hydrodynamic lubrication by water’, *Tribology International*. Elsevier, 75, pp. 31–38. doi: 10.1016/j.triboint.2014.03.009.

- Gertzog, K. P., Nikolakopoulos, P. G. and Papadopoulos, C. A. (2008) 'CFD analysis of journal bearing hydrodynamic lubrication by Bingham lubricant', *Tribology International*, 41(12), pp. 1190–1204. doi: 10.1016/j.triboint.2008.03.002.
- Jain, S. C., Sinhasan, R. and Singh, D. V. (1982) 'Elastohydrodynamic analysis of a cylindrical journal bearing with a flexible bearing shell', *Wear*, 78(3), pp. 325–335. doi: 10.1016/0043-1648(82)90243-5.
- Khonsari, M. M. and Wang, S. H. (1991) 'On The Fluid-Solid Interaction in Reference to Thermoelastohydrodynamic Analysis of Journal Bearings', *Journal of Tribology*, 113(2), pp. 398–404. doi: 10.1115/1.2920635.
- Lin, Q. *et al.* (2013) 'Analysis on the lubrication performances of journal bearing system using computational fluid dynamics and fluid-structure interaction considering thermal influence and cavitation', *Tribology International*. Elsevier, 64, pp. 8–15. doi: 10.1016/j.triboint.2013.03.001.
- Liu, H. *et al.* (2010) 'Application of Computational Fluid Dynamics and Fluid – Structure Interaction Method to the Lubrication Study of a Rotor – Bearing System', *Tribology Letters*, (123), pp. 325–336. doi: 10.1007/s11249-010-9612-6.
- Oh, K. P. and Huebner, K. H. (1973) 'Solution of the Elastohydrodynamic Finite Journal Bearing Problem', *Journal of Lubrication Technology*, 95(3), pp. 342–351.
- Okamoto, Y., Hanahashi, M. and Katagiri, T. (1999) 'Theoretical analysis of bearing considering elastic deformation - effects of the housing stiffness and bearing length on bearing performance', *JSAE Review*, 20(2), pp. 203–209.
- Raimondi, A. A. and Boyd, J. (1958a) 'A Solution for the Finite Journal Bearing and its Application to Analysis and Design: I', *A S L E Transactions*, 1(1), pp. 159–174. doi: 10.1080/05698195808972330.
- Raimondi, A. A. and Boyd, J. (1958b) 'A Solution for the Finite Journal Bearing and its Application to Analysis and Design: II', *A S L E Transactions*, 1(1), pp. 175–193. doi: 10.1080/05698195808972330.
- Raimondi, A. A. and Boyd, J. (1958c) 'A Solution for the Finite Journal Bearing and its Application to Analysis and Design: III', *A S L E Transactions*, 1(1), pp. 194–209. doi: 10.1080/05698195808972330.

Sfyris, D. and Chasalevris, A. (2012) ‘An exact analytical solution of the Reynolds equation for the finite journal bearing lubrication’, *Tribology International*. Elsevier, 55, pp. 46–58. doi: 10.1016/j.triboint.2012.05.013.

Versteeg, H. K. and Malalasekera, M. (2007) *An Introduction to Computational Fluid Dynamics: The Finite Volumes Method*. 2nd edn. Essex: Pearson Education Limited.

Wada, S., Hayashi, H. and Haga, K. (1974) ‘Behavior of a Bingham Solid in Hydrodynamic Lubrication : Part 3, Application to Journal Bearing’, *Bulletin of JSME*, 17(111), pp. 1182–1191. doi: 10.1248/cpb.37.3229.

Wodtke, M., Olszewski, A. and Wasilczuk, M. (2013) ‘Application of the fluid-structure interaction technique for the analysis of hydrodynamic lubrication problems’, *Proceedings of the Institution of Mechanical Engineers, Part J: Journal of Engineering Tribology*, 227(8), pp. 888–897. doi: 10.1177/1350650113481147.